ORIGINAL RESEARCH REPORT

Society For Biomaterials — WILEY

Extracellular matrix decorated polycaprolactone scaffolds for improved mesenchymal stem/stromal cell osteogenesis towards a patient-tailored bone tissue engineering approach

João C. Silva[1,2†] | Marta S. Carvalho[1,3†] | Ranodhi N. Udangawa[2] |
Carla S. Moura[4] | Joaquim M. S. Cabral[1] | Cláudia L. da Silva[1] |
Frederico Castelo Ferreira[1] | Deepak Vashishth[3] | Robert J. Linhardt[2,3]

[1]Department of Bioengineering and iBB-Institute for Bioengineering and Biosciences, Instituto Superior Técnico, Universidade de Lisboa, Lisbon, Portugal

[2]Department of Chemistry and Chemical Biology, Biological Sciences and Chemical and Biological Engineering, Center for Biotechnology and Interdisciplinary Studies, Rensselaer Polytechnic Institute, Troy, New York

[3]Department of Biomedical Engineering, Center for Biotechnology and Interdisciplinary Studies, Rensselaer Polytechnic Institute, Troy, New York

[4]CDRSP–Centre for Rapid and Sustainable Product Development, Polytechnic Institute of Leiria, Rua de Portugal-Zona Industrial, Marinha Grande, Portugal

Correspondence
Robert J. Linhardt, Department of Chemistry and Chemical Biology, Biological Sciences and Chemical and Biological Engineering, Center for Biotechnology and Interdisciplinary Studies, Rensselaer Polytechnic Institute, Troy, NY 12180-3590.
Email: linhar@rpi.edu

Abstract

The clinical demand for tissue-engineered bone is growing due to the increase of non-union fractures and delayed healing in an aging population. Herein, we present a method combining additive manufacturing (AM) techniques with cell-derived extra-cellular matrix (ECM) to generate structurally well-defined bioactive scaffolds for bone tissue engineering (BTE). In this work, highly porous three-dimensional poly-caprolactone (PCL) scaffolds with desired size and architecture were fabricated by fused deposition modeling and subsequently decorated with human mesenchymal stem/stromal cell (MSC)-derived ECM produced in situ. The successful deposition of MSC-derived ECM onto PCL scaffolds (PCL-MSC ECM) was confirmed after decellularization using scanning electron microscopy, elemental analysis, and immu-nofluorescence. The presence of cell-derived ECM within the PCL scaffolds significantly enhanced MSC attachment and proliferation, with and without osteogenic supplementation. Additionally, under osteogenic induction, PCL-MSC ECM scaffolds promoted significantly higher calcium deposition and elevated relative expression of bone-specific genes, particularly the gene encoding osteopontin, when compared to pristine scaffolds. Overall, our results demonstrated the favorable effects of combining MSC-derived ECM and AM-based scaffolds on the osteogenic differentiation of MSC, resulting from a closer mimicry of the native bone niche. This strategy is highly promising for the development of novel personalized BTE approaches enabling the fabrication of patient defect-tailored scaffolds with enhanced biological performance and osteoinductive properties.

[†]João C. Silva and Marta S. Carvalho contributed equally to this work.

1 | INTRODUCTION

The clinical demand for tissue-engineered bone has increased in recent years, due to numerous medical conditions that require clinical intervention in an aging population. Each year in the United States (US) alone, ~8 million people develop fractures, of which 5–10% fail to heal under standard treatment, resulting in non-union fractures (Holmes, 2017). The most common clinical procedures available to address these needs still rely on autologous and allogeneic bone grafts, however, these approaches are accompanied by side effects, and are limited for a wide-scale application due to the scarcity of the grafts (Chiarello et al., 2013). Therefore, new promising solutions for bone repair are being developed. In particular, bone tissue engineering (BTE) offers the possibility of generating new bone tissue by combining stem cells or osteoprogenitor cells, differentiation-inducing molecules, and three-dimensional (3D) biomaterial scaffolds, with great promise of improvements in tissue functionality. However, despite an extensive amount of research on BTE and the recent technological developments in bio-material science, challenges still remain in achieving functional and mechanically competent bone growth (Gordeladze, Haugen, Lyngstadaas, & Reseland, 2017).

Personalized medicine in bone repair may follow a patient-tailored approach in which bioengineered products are customized to perfectly fit the shape, structure, and dimensions of the defect site within the bone of a patient. Additionally, cells isolated from the patient can be further integrated in this personalized BTE approach, representing an autologous strategy that reduces risk of immune rejection and inflammation (Neves, Rodrigues, Reis, & Gomes, 2016; Roseti et al., 2017). The success of the implementation of BTE approaches in personalized medicine is highly dependent on the development of high-precision equipment for the automated, repro-ducible, and scalable production of functional bone tissue constructs.

Additive manufacturing (AM) techniques such as fused deposition modeling (FDM) and 3D printing have been used to fabricate scaffolds for BTE applications, offering advantages in controlling scaffold structural properties such as pore size, porosity and mechanical strength (Roseti et al., 2017). Additionally, AM techniques can be successfully implemented in personalized BTE by acquiring bone defect data and generating a 3D Computer Aided Design (CAD) model of both the anatomical structure in the patient and of the biomaterial scaffold for implantation in the defect site. Based on these CAD models, a precise scaffold can be manufactured, seeded with cells and placed into the patient's defect to promote bone regeneration (Figure 1) (Melchels

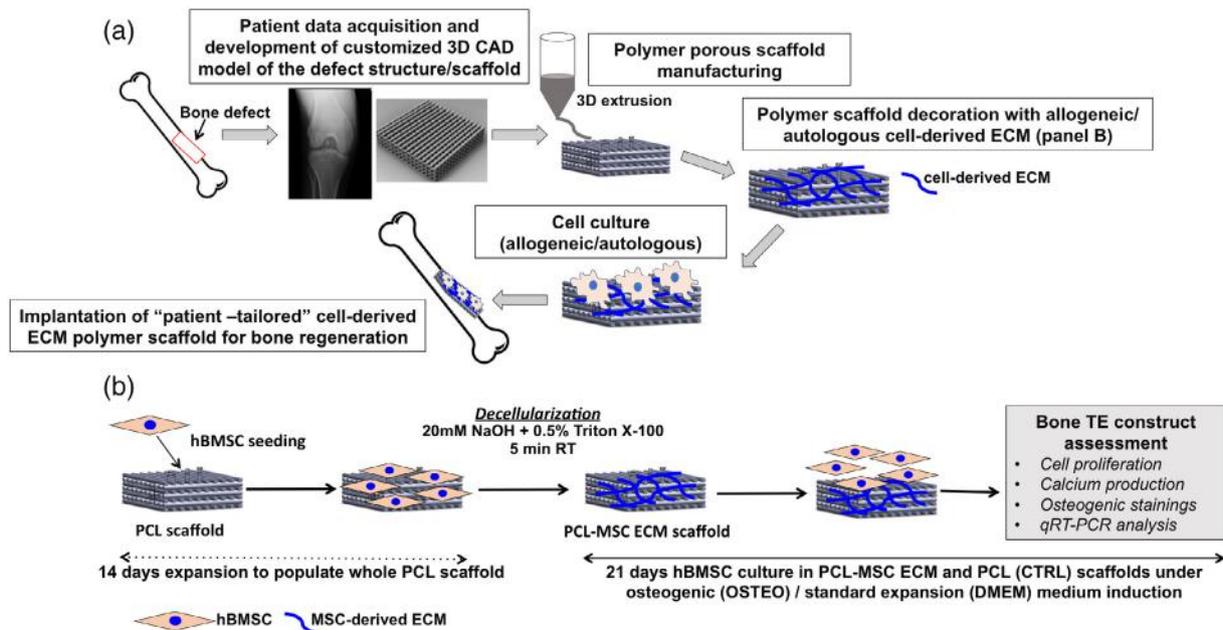**FIGURE 1** (a) Schematic representation of a personalized patient-tailored bone tissue engineering approach combining additive manufacturing of polymer scaffolds and subsequent decoration with cell-derived ECM to improve scaffold's biological performance. (b) Scheme of the experimental plan for the generation of PCL-MSC ECM scaffolds and evaluation of their ability to promote MSC proliferation and osteogenic differentiation

et al., 2012; Mota, Puppi, Chiellini, & Chiellini, 2015). FDM-based BTE scaffolds are produced using thin thermoplastic filaments or granules that are melted by heating and guided by a robotic device with computer-controlled motion to generate the desired structures (Domingos et al., 2012; Melchels et al., 2012). FDM often works with easy to process, biodegradable and biocompatible synthetic polymers such as polycaprolactone (PCL) or polylactic acid (PLA). These materials, alone or in combination with osteoinductive minerals, have been widely applied in BTE approaches (Hajiali, Tajbakhsh, & Shojaei, 2018; Hutmacher et al., 2001; Poh et al., 2016; Roseti et al., 2017). The US Food and Drug Administration (FDA) has approved PCL-based scaffolds fabricated by FDM for craniofacial applications after their performance was demonstrated in clinical pilot studies (Low, Ng, Yeo, & Chou, 2009; Schantz et al., 2006). PCL scaffolds have been extensively used to regenerate hard tissues like bone due to their mechanical properties and slow biodegradation rate. However, this synthetic material lacks bioactive sites and proteins, which hampers cell attachment and differentiation (Benders et al., 2013).

Different strategies have been employed to improve the biological response and osteoinductive properties of scaffolds through a better mimicry of the bone ECM. Such approaches include modification of the scaffold's surface with ECM components (e.g., collagen, fibronectin and vitronectin) (Ku, Chung, & Jang, 2005; Kundu & Putnam, 2006; Won et al., 2015) or the introduction of cell-binding motifs, such as Arg-Gly-Asp (RGD) peptide (Guler, Silva, & Sezai Sarac, 2017). However, these proteins and peptides are not easily processed within the scaffold material and often fail to achieve the molecular complexity of the native ECM. While decellularized tissue-ECM scaffolds can more closely mimic tissue complexity, their application in BTE is limited by the fast degradation, weak mechanical properties, potential pathogen transfer, and source tissue variability and scarcity (Bracaglia & Fisher, 2015; Hoshiba, Lu, Kawazoe, & Chen, 2010).

Cell-derived ECM is a promising alternative approach as it serves as a reservoir of multiple cytokines and growth factors, providing a close mimicry of the physical and chemical cues present in the in vivo microenvironment (Fitzpatrick & McDevitt, 2015; Hynes, 2009). In these approaches, cells are cultured in vitro until confluence, allowing for the secretion and accumulation of ECM components and then exposed to a decellularization protocol to generate cell-derived ECM. Decellularization has been performed through chemical, physical, or combined methods (Fernández-Pérez & Ahearne, 2019; Hoshiba et al., 2010). During this process, cells and genetic material are removed while the structure, architecture, and protein composition of the ECM should be maintained (Fitzpatrick & McDevitt, 2015). Moreover, ECM is insoluble and has a highly stable core structure, allowing the extraction of cellular components while leaving an interconnected fibrillar network of ECM components. Decellularized cell-derived ECM is composed of different types, amounts and distributions of proteins, which interact with different cell types, influencing several cellular processes (Harris, Raitman, & Schwarzbauer, 2018). Additionally, by using cultured cells specifically selected to mimic an intended niche, decellularized cell-derived ECM allows for a higher degree of customization in comparison to tissue-derived ECM (Choi, Choi, Woo, & Cho, 2014; Gattazzo, Urciuolo, & Bonaldo, 2014).

Decellularized ECM from mesenchymal stem/stromal cells (MSC) has been able to promote MSC proliferation and osteogenic differentiation (Carvalho, Silva, Cabral, da Silva, & Vashishth, 2019; Lai et al., 2010). Autologous or allogeneic cell-derived ECM can also be deposited in 3D synthetic scaffolds to generate constructs with improved cellular activities, resulting in a closer mimicry of the native niche while maintaining adequate structural and mechanical properties (Cheng, Solorio, & Alsberg, 2014; Hoshiba et al., 2010). In fact, 3D cell-derived ECM scaffolds have been developed by cell-derived ECM deposition on different organic and inorganic materials. Cell-derived ECM–PCL electrospun scaffolds (Carvalho et al., 2019; Thibault, Scott Baggett, Mikos, & Kasper, 2010)—titanium implants (Datta, Holtorf, Sikavitsas, Jansen, & Mikos, 2005) and—ceramic scaffolds (Kim, Ventura, & Lee, 2017; Tour, Wendel, & Tcacencu, 2011) have been previously applied in BTE approaches and demonstrated a clear improvement in scaffold's bioactivity and osteogenic properties.

The aim of this study was to develop extrusion-based 3D porous PCL scaffolds with controlled architecture, high porosity, and high interconnectivity, and decorate them with human bone marrow MSC—derived ECM produced in situ. Our hypothesis is that by providing a scaffold with good mechanical support and containing MSC-derived ECM environmental cues, we could create an in vitro platform with a closer mimicry of the in vivo bone ECM. The in vitro niche produced would then be capable of promoting different cellular processes, such as cell attachment, proliferation, and osteogenic differentiation. Therefore, this study presents a method to enhance the bioactivity and osteoinductivity of AM-based synthetic scaffolds through a closer recreation of native-like structural, chemical, and physical signals provided by the decellularized MSC-ECM. The MSC-derived ECM PCL scaffolds developed herein were characterized in terms of their structure and presence of ECM components. Additionally, their ability to promote the osteogenic differentiation of human MSC in comparison to pristine PCL scaffolds was evaluated by assessing cell proliferation, calcium production, typical osteogenic stainings, and bone marker genes expression.

2 | MATERIALS AND METHODS

2.1 | Cell culture

Human bone marrow MSC (hBMSC) were obtained from Lonza (Basel, Switzerland). hBMSC were thawed and plated at a cell density of 3,000 cells/cm^2 on tissue culture flasks (CELLTREAT® Scientific Products, MA) using low-glucose Dulbecco's Modified Eagle Medium (DMEM, Gibco, Grand Island, NY) supplemented with 10% fetal bovine serum (FBS, Gibco) and 1% penicillin–streptomycin (Pen-strep, Gibco), and kept at 37°C and 5% CO_2 in a humidified atmosphere. Medium renewal was performed every 3–4 days. All the experiments were performed using cells with passage numbers between 3 and 5.

2.2 | Fabrication of 3D extruded porous PCL scaffolds

PCL (MW 50000 Da, CAPA™ 6500, Perstorp Caprolactones, UK) scaffolds were fabricated in a layer-by-layer approach using an in-house developed FDM equipment, the Bioextruder, as previously reported in the literature (Domingos et al., 2012; Silva, Moura, Alves, Cabral, & Ferreira, 2017). Briefly, the PCL filament material was heated at 80°C (a temperature above PCL's melting point of 60°C) and extruded through a nozzle guided by a robotic device with computer-controlled motion. PCL scaffolds with the desired size, structure, and architecture, and with a selected 0–90° lay-down pattern were obtained in accordance with the 3D models designed in CAD software (SolidWorks, Dassault Systèmes).

2.3 | Generation of cell-derived ECM decorated PCL scaffolds

Prior to cell culture, PCL scaffolds were sterilized by ultraviolet radiation exposure (1 hr each side of the scaffold), and through 70% ethanol washing. Afterwards, the scaffolds were rinsed three times with phosphate buffered saline (PBS, Gibco) + 1% Pen-strep solution and incubated with culture media for 1 hr. MSC-derived ECM decorated PCL scaffolds (PCL-MSC ECM) were generated by a pre-culture of hBMSC on the PCL scaffolds followed by complete scaffold decellularization (Figure 1a). hBMSC were harvested and seeded onto the PCL scaffolds (1.2×10^5 cells/scaffold) and placed in an ultra-low attachment 24-well plate (Corning, NY). The scaffolds were then incubated for 2 hr without culture media to allow initial cell attachment. Standard MSC growth medium consisting of DMEM + 10% FBS + 1% Pen-strep was added to each scaffold and the culture medium was changed every 3–4 days. After 14 days of culture to allow for hBMSC growth and migration through the entire scaffold, the medium was discarded and the scaffolds were rinsed twice with PBS. Afterwards, the cell-scaffold samples were decellularized following a previously reported protocol (Kang, Kim, Bishop, Khademhosseini, & Yang, 2012; Matsubara et al., 2004) by exposure to a 20 mM ammonium hydroxide (NH_4OH) + 0.5% Triton X-100 (Sigma-Aldrich, St. Louis, MO) solution for 5 min at room temperature. The ECM decorated PCL scaffolds were then gently washed three times with PBS. Samples were collected for immunofluorescence staining, scanning electron microscopy (SEM) and elemental analysis, as described in the following sections, to confirm the efficiency of the decellularization protocol.

2.4 | Characterization of cell-derived ECM decorated PCL scaffolds

2.4.1 | Immunofluorescent staining

The efficiency of scaffold decellularization treatment was assessed by cell morphology/immunocytochemistry analysis before and after decellularization. Thus, scaffolds were washed twice with PBS, fixed with 4% paraformaldehyde (PFA; Santa Cruz Biotechnology, Dallas, TX) for 20 min and then permeabilized with 0.1% Triton X-100 for 10 min. Afterwards, scaffolds were incubated with phalloidin (dilution 1:250–2 μg/ml, Sigma) for 45 min in the dark, washed twice with PBS and counterstained with 4,6-diamino-2-phenylindole (DAPI, 1.5 μg/ml, Sigma) for 5 min. After washing twice with PBS, scaffolds before and after the decellularization process were imaged by fluorescent microscopy (Olympus IX51 Inverted Microscope: Olympus America Inc., Melville, NY).

Immunofluorescent staining for fibronectin and laminin was performed to investigate the presence of relevant ECM protein components and their distribution pattern on the decellularized ECM decorated PCL scaffolds. Therefore, PCL-MSC ECM scaffolds were washed with PBS and fixed with 4% PFA for 20 min at room temperature. Then, the scaffolds were washed three times with 1% bovine serum albumin (BSA) in PBS for 5 min. PCL-MSC ECM scaffolds were permeabilized and blocked with a solution of 0.3%Triton X-100, 1% BSA and 10% donkey serum in PBS at room temperature for 45 min, and incubated overnight at 4°C with mouse anti-human primary antibodies for laminin and fibronectin (10 μg/ml in 0.3% Triton X-100, 1% BSA, 10% donkey serum solution) (R&D systems, Minneapolis, MN). After washing with 1% BSA in PBS, a NorthernLights™ 557-conjugated anti-mouse IgG secondary antibody (dilution 1:200 in 1% BSA PBS) (R&D systems) was added to the samples and incubated in the dark for 1 hr at room temperature. Finally, cell nuclei were counterstained with DAPI (1.5 μg/ml, Sigma) for 5 min and the scaffolds were washed with PBS. The immunofluorescence staining was observed by fluorescence microscopy.

2.4.2 | SEM analysis

Prior to imaging, scaffold samples were fixed with 4% PFA for 20 min, washed thoroughly with PBS and dehydrated sequentially in 20, 40, 60, 80, 95, and 100% (vol/vol) ethanol solutions for 20 min each. Then, samples were mounted on a holder and sputter-coated with a thin layer of 60% gold–40% palladium. The morphological and structural characterization of the PCL-MSC ECM and PCL scaffolds was performed using a field emission scanning electron microscope (FE-SEM, FEI-Versa 3D Dual Beam, Hillsboro). Samples were imaged at several magnifications using an accelerating voltage of 3 kV.

2.4.3 | Energy dispersive X-ray analysis

Carl Zeiss Supra field emission scanning electron microscope (FESEM, Hillsboro, OR) was used to conduct energy dispersive X-ray (EDX) analysis on the pristine PCL and PCL-MSC ECM scaffolds. The analysis was performed using an acceleration voltage of 10 kV and a spot size of 120 μm. The presence of specific elements on the EDX spectra of each sample was analyzed using INCA Microanalysis Suite software.

2.5 | Effects of PCL-MSC ECM scaffolds on the proliferation and osteogenic differentiation of hBMSC

2.5.1 | hBMSC seeding, proliferation, and differentiation on PCL-MSC ECM scaffolds

hBMSC were seeded on PCL-MSC ECM and PCL scaffolds (control) at a density of 1×10^5 cells per scaffold and incubated for 2 hr at 37°C/5% CO_2 before adding culture media to promote initial cell attachment. In order to assess the effects of MSC-ECM presence on the biological performance and osteoinductive capacity of PCL scaffolds, four different experimental groups were considered: (a) PCL DMEM and (b) PCL-MSC ECM DMEM scaffold groups were cultured under standard expansion media consisting of DMEM supplemented with 10% FBS + 1% Pen-strep, while (c) PCL OSTEO and (d) PCL-MSC ECM OSTEO scaffold groups were cultured with osteogenic differentiation medium, composed by DMEM supplemented with 10% FBS, 10 mM β-glycerophosphate (Sigma-Aldrich), 10 nM dexamethasone (Sigma-Aldrich), 50 μg/ml ascorbic acid (Sigma-Aldrich) and 1% Pen-strep. Scaffold-cell constructs of the different experimental groups were cultured during 21 days and medium renewal was performed every 3–4 days.

2.5.2 | Cell viability and proliferation assay

The metabolic activity of hBMSC in the different experimental scaffold groups was evaluated on days 1, 7, 14, and 21 using AlamarBlue® cell viability reagent (ThermoFischer Scientific, Waltham, MA) following the manufacturer's guidelines. Briefly, a 10% vol/vol AlamarBlue® solution in culture medium was added to the scaffolds and incubated at 37°C in 5% CO_2 chamber for 3 hr. Fluorescence intensity was measured in a microplate reader (SpectraMax M5, Molecular Devices) at an excitation/emission wavelength of 560/590 nm and compared to a calibration curve to assess the equivalent number of cells present in each scaffold. Scaffolds without seeded cells (for each experimental group) were used as blank controls in the fluorescence intensity measurements. Four scaffolds (n = 4) were analyzed for each experimental group and fluorescence values of each sample were measured in triplicate.

2.5.3 | SEM and EDX analysis

The morphology of hBMSC after 21 days of culture on PCL-MSC ECM and PCL scaffolds under the four different experimental conditions was analyzed by SEM. Fixed cell-scaffold constructs were stained with 1% (vol/vol) osmium tetroxide (Sigma-Aldrich) solution for 30 min and washed twice with PBS. Afterwards, samples were dehydrated using ethanol gradient solutions (20, 40, 60, 80, 95, and 100% [vol/vol]) for 20 min each and finally dried in a critical point dryer (supercritical Automegasamdri 915B, Tousimis) in 100% isopropanol. Dried samples were then mounted, sputter-coated and imaged using the above-mentioned procedure. EDX analysis was performed using the parameters specified in the previous section to assess for calcium deposition (typical marker of osteogenic differentiation) by hBMSC cultured for 21 days under the different experimental conditions.

2.5.4 | Calcium quantification assay

Calcium content quantification was performed after 14 and 21 days of hBMSC-scaffold culture for the four different experimental groups. Samples were washed with PBS and incubated with a 6 M hydrochloric acid (HCl) solution (Sigma-Aldrich) under agitation overnight at 4°C to remove and dissolve the calcium. The supernatant was then collected and used for calcium determination according to the manufacturer's instructions of the calcium colorimetric assay kit (Sigma-Aldrich). Absorbance at 575 nm was measured for each scaffold on a plate reader (SpectraMax M5, Molecular Devices), and normalized to the total number of cells. Note that acellular scaffolds for each experimental group were used as blank controls. Three scaffolds (n = 3) were analyzed for each condition and absorbance values of each sample were measured in triplicate. Finally, the absorbance values obtained for each blank control were subtracted from the respective sample group and total calcium was calculated using a calcium standard calibration curve.

2.5.5 | Osteogenic staining

After 21 days of culture, samples from the different experimental groups were assessed for osteogenic differentiation using alkaline phosphatase (ALP)/Von Kossa and Xylenol Orange stainings. For the ALP staining, culture medium was removed, samples were washed once with PBS, and fixed with 4% PFA for 20 min. Afterward, samples were rinsed in miliQ water during 5 min and incubated with Fast Violet solution (Sigma-Aldrich) and Naphthol AS-MX Phosphate Alkaline solution (Sigma-Aldrich) in a final concentration of 4% for 45 min at room temperature in the dark. In the case of Von Kossa staining, the scaffolds were washed twice with miliQ water and incubated with 2.5% silver nitrate solution (Sigma-Aldrich) for 30 min at room temperature protected from light. Finally, samples were washed three times with miliQ water and imaged using a fluorescence microscope (Olympus IX51 Inverted Microscope, NY). A 20 mM volume of Xylenol Orange solution (Sigma-Aldrich) was added to previously fixed samples and incubated for 1 hr at room temperature in the dark to visualize the mineral deposits formed after hBMSC osteogenic differentiation on PCL and PCL-MSC ECM scaffolds. Scaffolds were then washed three times with PBS and twice with miliQ water and the fluorescent staining was observed using a fluorescence microscope.

2.5.6 | RNA extraction and quantitative real-time PCR analysis

Total RNA was extracted using the RNeasy Mini Kit (QIAGEN, Hilden, Germany). The scaffolds were first incubated in lysis buffer with

200 rpm agitation for 1 hr at 4°C. Afterward, total RNA was isolated according to the manufacturer's protocol and quantified using a Nanodrop (ND-1000 Spectrophotometer, Nanodrop Technologies). cDNA was synthesized from the purified RNA using iScript™ Reverse Transcription Supermix (Bio-Rad, Hercules, CA) according to manufacturer's guidelines. Reaction mixtures (20 μl) were incubated in a thermal cycler (Veriti Thermal Cycler, Applied Biosystems, CA) with the following temperature protocol: 5 min at 25°C, 20 min at 46°C and 1 min at 95°C. The quantitative reverse transcription-polymerase chain reaction (qRT-PCR) was performed using PowerUp SYBR® Green Master Mix (Applied Biosystems) and the StepOnePlus real-time PCR equipment (Applied Biosystems). All reactions were carried out in accordance with the manufacturer's guidelines and using the following temperature protocol: denaturation step at 95°C for 10 min, followed by 40 cycles of 95°C (amplification step) for 15 s and 60°C for 1 min (annealing and extension). All samples were assayed in triplicate and the results were analyzed using the $2^{-\Delta\Delta Ct}$ method. Target genes (collagen type I (*COL I*), runt-related transcription factor (*Runx2*), alkaline phosphatase (*ALP*) and osteopontin (*OPN*)) expression was primarily normalized to the housekeeping gene glyceraldehyde 3-phosphate dehydrogenase (*GAPDH*) and then determined as a fold-change relative to the baseline expression of the target genes measured in the PCL scaffolds in DMEM (PCL DMEM). The primer sequences used in the qRT-PCR analysis are summarized in Table 1.

2.6 | Statistical analysis

Results are presented as mean values ± *SD*. Each experiment was conducted in triplicate (*n* = 3), unless specified differently. The statistical analysis of the data was performed using one-way ANOVA, followed by Tukey post hoc test. GraphPad Prism version 7 software was used in the analysis and differences were considered to be significant when *p*-values obtained were less than 0.05 (95% confidence intervals) (*p < .05, **p < .01, ***p < .001).

3 | RESULTS

3.1 | Cell-derived ECM decorated PCL scaffolds production and characterization

The efficiency of the decellularization method used to generate MSC-derived ECM on PCL scaffolds was assessed and is presented in Figure 2. Prior to decellularization treatment, immunofluorescence staining of F-actin labeled by phalloidin in red and nucleus labeled by DAPI in blue confirmed the presence of well-defined cell nuclei distributed throughout the scaffold (Figure 2a,c). After decellularization by exposure to a 20 mM NH$_4$OH in 0.5% Triton X-100 solution, the residual DAPI staining (Figure 2b) indicated that most of the cellular nuclei were disrupted, confirming the efficiency of decellularization. The presence of ECM protein components on the PCL scaffolds after decellularization was demonstrated by immunofluorescent staining of fibronectin (Figure 2d) and laminin (Figure 2e).

The PCL-MSC ECM scaffolds were also analyzed by SEM and EDX and compared to the pristine PCL scaffolds (Figure 3). In contrast to the smooth regular surface observed in pristine PCL scaffold (Figure 3a,b—top view/E and F-side view), SEM micrographs showed clearly the presence of cell-derived ECM on the surface of the PCL-MSC ECM scaffold (Figure 3c,d—top view) and (Figure 3g,h—side view). The EDX spectra (Figure 3i,j) showed that, compared to PCL pristine scaffold, PCL-MSC ECM scaffold contained nitrogen, in addition to the carbon and oxygen constituents of PCL. In combination with SEM (Figure 3) and fibronectin/laminin immunofluorescence staining (Figure 2d,e), this result demonstrates the presence of ECM components on PCL-MSC ECM scaffolds after the decellularization treatment.

3.2 | Effects of PCL-MSC ECM scaffolds on cell proliferation

The metabolic activity of hBMSC cultured on PCL-MSC ECM and PCL scaffolds with standard expansion medium (DMEM+10% FBS) and osteogenic differentiation medium was measured by AlamarBlue® assay throughout the 21 days of culture and converted to equivalent cell numbers to assess the effect of MSC-derived ECM deposited onto PCL scaffolds on cell proliferation (Figure 4). After the first day of culture, PCL-MSC ECM scaffolds presented a higher equivalent number of cells compared to pristine PCL scaffolds, suggesting that MSC-derived ECM had a positive impact on cell adhesion. A statistically significant (*p* < .05) increase in cell number was obtained when cells were cultured on PCL-MSC ECM scaffolds compared to pristine PCL scaffold under expansion media. At day 7, cells cultured on PCL-MSC ECM scaffolds reached higher and statistically significant (*p* < .001) equivalent cell numbers compared with PCL scaffolds both under standard expansion and osteogenic differentiation media, demonstrating the efficiency of PCL-MSC ECM scaffolds in promoting cell

Gene	Fwd sequence	Rev sequence
GAPDH	5′-AACAGCGACACCCACTCCTC-3′	5′-CATACCAGGAAATGAGCTTGACAA-3′
COL I	5′-CAT CTC CCC TTC GTT TTT GA-3′	5′-CCA AAT CCG ATG TTT CTG CT-3′
Runx2	5′-AGATGATGACACTGCCACCTCTG-3′	5′-GGGATGAAATGCTTGGGAACT-3′
ALP	5′-ACCATTCCCACGTCTTCACATTT-3′	5′-AGACATTCTCTCGTTCACCGCC-3′
OPN	5′-TGTGAGGTGATGTCCTCGTCTGTAG-3′	5′-ACACATATGATGGCCGAGGTGA-3′

TABLE 1 Forward and reverse primer gene sequences used in qRT-PCR analysis

FIGURE 2 Characterization of the decellularization process to generate PCL-MSC ECM scaffolds. Fluorescence images of DAPI/Phalloidin staining before (a, c) and after (b) scaffold treatment with 20 mM NaOH +0.5% Triton X-100 solution confirm the efficiency of the decellularization method used. The presence of ECM protein components Fibronectin (d) and Laminin (e) on PCL-MSC ECM scaffolds was confirmed by immunofluorescence staining. DAPI stains cell nuclei blue and phalloidin stains Actin-rich cell cytoskeleton red. Scale bar 100 μm
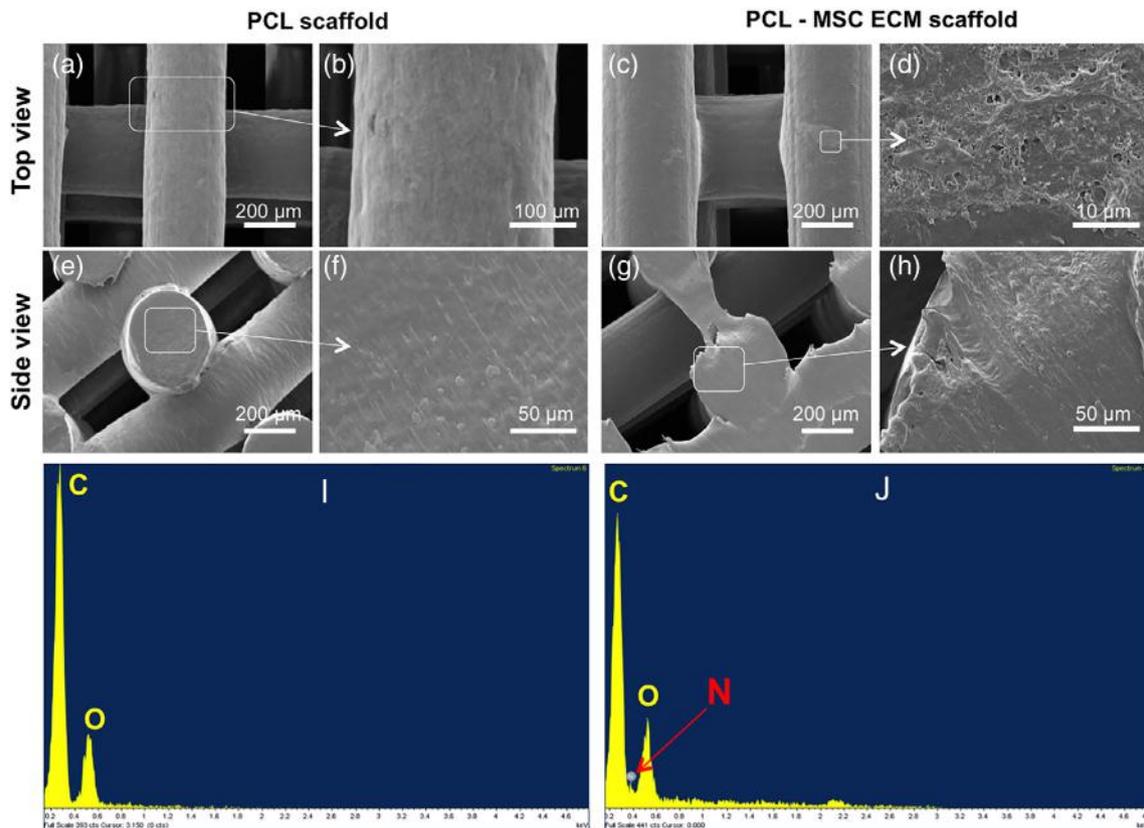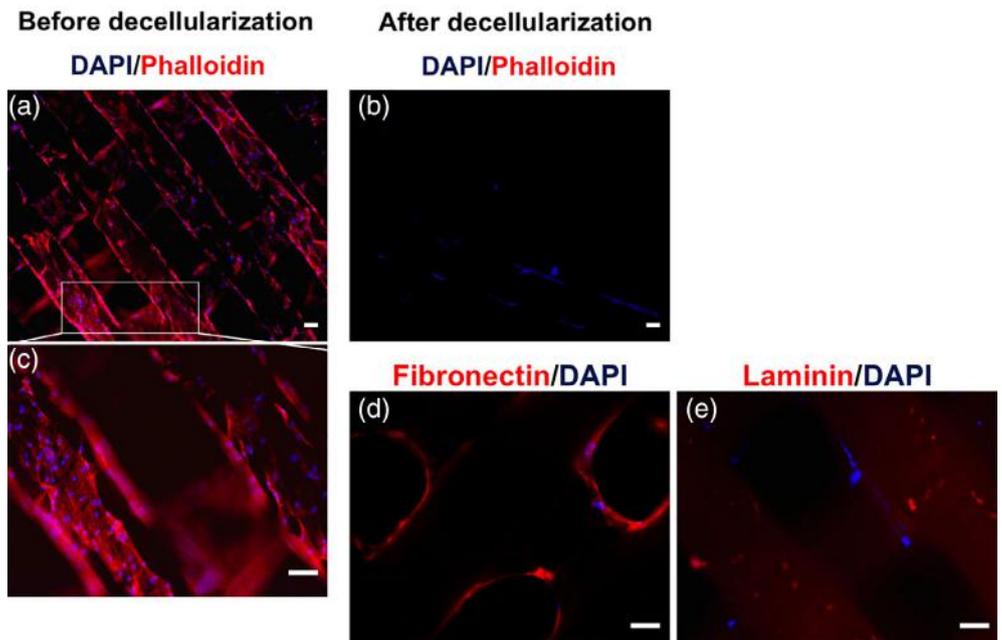

FIGURE 3 SEM morphological analysis of PCL (a, b, e, and f) and PCL-MSC ECM (c, d, g, and h) scaffolds. The absence/presence of MSC-derived ECM in the PCL scaffold (pristine PCL vs. PCL-MSC ECM) was confirmed by top view (a, b/c, d) and side view (e, f/g, h) SEM micrographs, respectively. EDX spectrograms of pristine PCL (i) and PCL-MSC ECM scaffold (j). The nitrogen peak identified in PCL-MSC ECM spectrogram (j) suggests the presence of cell-derived ECM in addition to PCL material. The inserts (white box) in the images a, c, e, and g identify the scaffold region that is showed in a higher magnification in images b, d, f, and h, respectively. Scale bars values of SEM micrographs are depicted in the figure

proliferation. Cell proliferation was steeply up to day 14 and the number of cells increased continuously during incubation in all experimental groups during the 21 days of culture. Significant differences in cell numbers between PCL-MSC ECM scaffolds and their pristine PCL counterparts were evident throughout culture (Figure 4). These results clearly demonstrated that the deposition of decellularized ECM onto

PCL scaffolds enhanced hBMSC attachment and proliferation, both under expansion and osteogenic differentiation induction.

3.3 | Osteogenic gene expression

qRT-PCR analysis was performed to assess bone-specific gene expression after hBMSC culture on PCL-MSC ECM scaffolds (Figure 5). hBMSC cultured on PCL-MSC ECM scaffolds without osteogenic induction (DMEM) showed significantly higher expression of *COL I* ($p < .01$) (Figure 5a), *Runx2* ($p < .001$) (Figure 5b) and *ALP* ($p < .01$) (Figure 5c) genes after 21 days compared with MSC cultured on pristine PCL scaffolds. Interestingly, hBMSC cultured on PCL-MSC ECM DMEM demonstrated statistically significant ($p < .01$) higher expression levels of *COL I* and *Runx2* compared with hBMSC cultured on

osteogenic differentiation medium on pristine PCL scaffolds and similar to the ones verified for PCL-MSC ECM OSTEO group. These results suggest that the incorporation of MSC-derived ECM onto PCL scaffolds produced an effect powerful enough to support alone (i.e., in the absence of osteogenic inductive soluble factors) the upregulation of certain osteogenic genes expression levels to values higher than the ones expressed by hBMSC cultured on pristine PCL scaffolds under osteogenic induction medium.

Importantly, a statistically significant ($p < .01$) enhancement in *OPN* gene expression (Figure 5d) was only observed when hBMSC were cultured under osteogenic differentiation conditions onto PCL-MSC ECM scaffolds. These data illustrate that MSC-derived ECM combined with PCL scaffolds can enhance osteogenesis, compared to PCL pristine scaffolds as suggested by the higher mRNA expression levels of *Col I*, *Runx2*, *ALP*, and *OPN* (Figure 5).
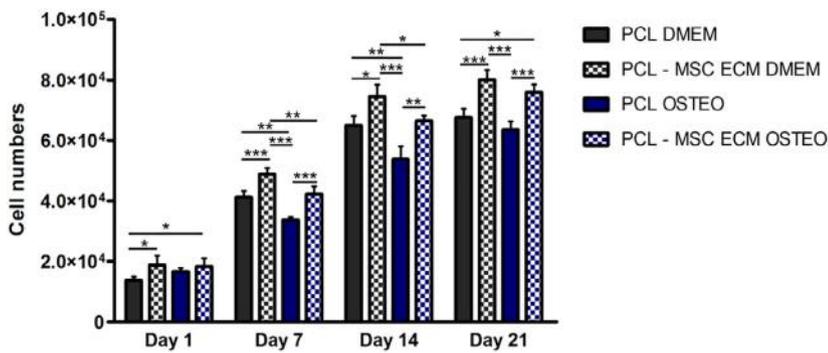
FIGURE 4 Proliferation of hBMSC cultured on PCL-MSC ECM and pristine PCL scaffolds for 21 days under standard DMEM +10% FBS medium and osteogenic differentiation medium. Results are expressed as mean ± *SD*; *n* = 4; *$p < .05$, **$p < .01$, ***$p < .001$
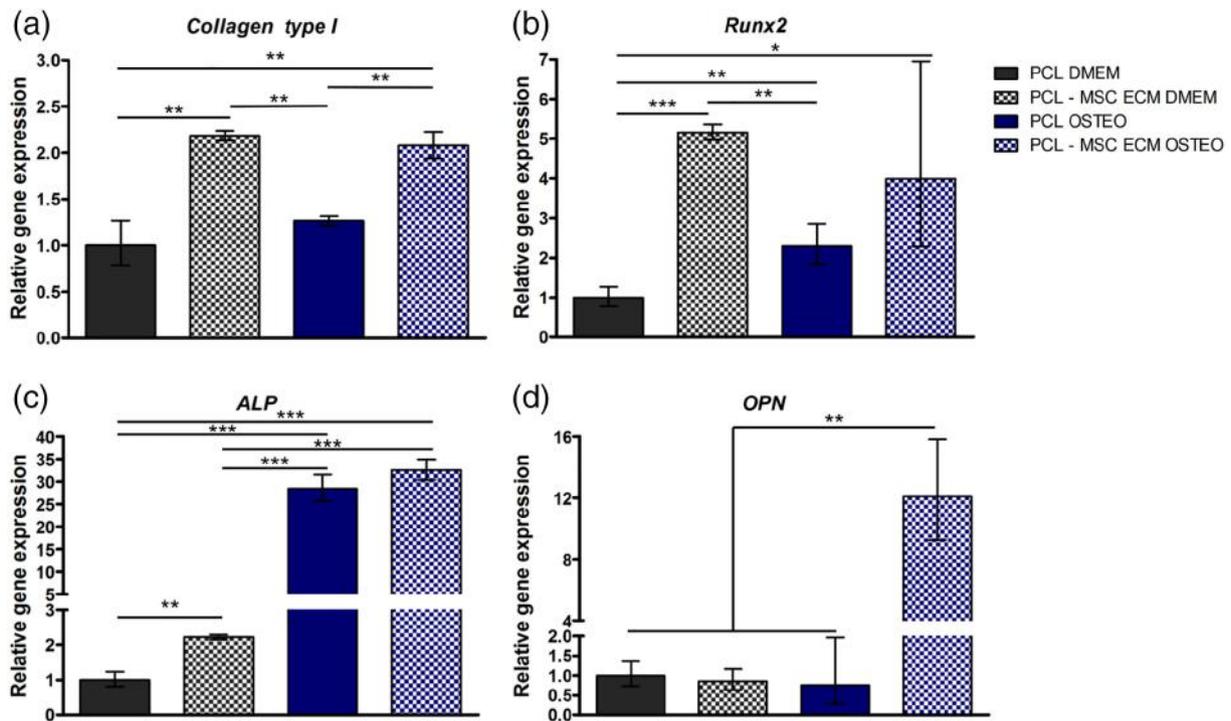
FIGURE 5 Osteogenic marker gene expression analysis by quantitative real-time PCR after 21 days of MSC culture on PCL-MSC ECM/PCL scaffolds under osteogenic differentiation medium and standard expansion medium. Expressions of (a) *Collagen type I*, (b) *Runx2*, (c) *ALP*, and (d) *OPN* were normalized to the endogenous gene *GAPDH* and calculated as a fold-change relative to the baseline expression of target gene measured in the PCL DMEM experimental group. Results are expressed as mean ± *SD*; *n* = 3; *$p < .05$, **$p < .01$, ***$p < .001$

3.4 | Effects of PCL-MSC ECM scaffolds on mineralization and bone ECM production

SEM morphological evaluation of the final tissue constructs obtained after 21 days of hBMSC culture on PCL-MSC ECM and pristine PCL scaffolds with and without osteogenic induction demonstrated the presence of cells surrounded by secreted ECM (Figure 6a–h). However, the presence of mineralized particles was more evident on the constructs cultured under osteogenic induction. Additionally, EDX analysis (Figure 6i–l) of the different experimental groups confirmed the presence of calcium element in the PCL-MSC ECM (Figure 6l) and PCL (Figure 6k) scaffolds when cultured in osteogenic induction medium.

ALP/Von Kossa and Xylenol Orange staining were performed to evaluate the hBMSC osteogenic differentiation on PCL-MSC ECM and pristine PCL scaffolds. ALP (Figure 7b–e) and Von Kossa (Figure 7f–i) staining confirmed ALP activity (red areas, Figure 7d,e) as well as the presence of mineral deposits (darker regions highlighted by white arrows in Figure 7h,i), in all scaffolds cultured in osteogenic differentiation media. Interestingly, the amount of mineral deposits observed increased considerably in PCL-MSC ECM OSTEO group (Figure 7i). Xylenol Orange fluorescent stain was used to further observe the mineralized deposits of calcium produced by hBMSC cultured on PCL-MSC ECM and PCL scaffolds (Figure 7j–m). When hBMSC were cultured on both scaffolds (with and without ECM) under standard expansion medium, few deposits of calcium were observed surrounding the construct (Figure 7j,k). Although no dramatic differences between cells cultured onto PCL

and PCL-MSC ECM scaffolds were observed after 21 days using Xylenol Orange stain (Figure 7l,m), these results demonstrate that osteogenic induction promoted the increase of calcium deposition by hBMSC. Therefore, this qualitative data confirmed the successful differentiation of hBMSC into osteoblasts in both PCL-MSC ECM and pristine PCL scaffolds when cultured in osteogenic differentiation medium.

Calcium content (Figure 7a) was also assessed after 14 and 21 days of culture under different experimental conditions to evaluate the effects of PCL-MSC ECM scaffolds on mineralization. After 14 days, the amount of cell-secreted calcium of cells cultured onto PCL-MSC ECM and PCL scaffolds under osteogenic medium induction was significantly increased compared to their respective scaffold counterparts cultured under expansion conditions. In fact, the amount of calcium produced by cells cultured onto PCL scaffolds was higher than the value observed for PCL-MSC ECM scaffolds when both were cultured under osteogenic induction conditions, however this difference was not statistically significant. As expected, hBMSC cultured 21 days on PCL-MSC ECM and PCL scaffolds under osteogenic differentiation medium produced significantly higher calcium levels compared with hBMSC cultured on scaffolds under expansion conditions. Moreover, under expansion conditions, the presence of MSC-ECM on the PCL scaffolds demonstrated no effect on calcium production. Importantly, under osteogenic differentiation medium, cells cultured in PCL-MSC ECM produced significantly ($p < .05$) more calcium when compared to pristine PCL scaffold, suggesting that ECM deposition on PCL scaffolds might enhance mineralization by hBMSC after osteogenic induction. These results are concordant with the observations
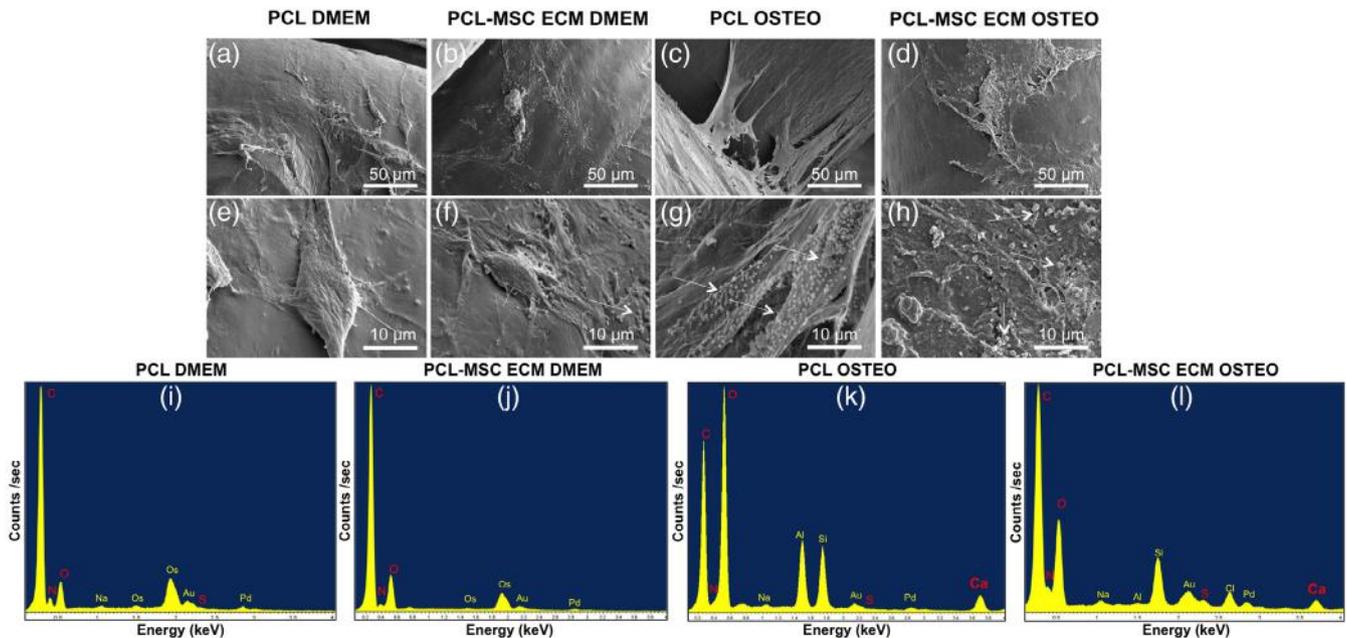

FIGURE 6 (a–h) SEM images at two different magnifications of MSC cultured on PCL-MSC ECM and pristine PCL scaffolds for 21 days under osteogenic differentiation media and standard expansion media. White arrows highlight the presence of mineralized nodules after 21 days of culture on PCL-MSC ECM/PCL scaffolds. (i–j) EDX spectrograms obtained after analysis of the different sample groups confirm the presence of calcium secreted by cells cultured on PCL-MSC ECM/PCL scaffolds exposed to osteogenic medium induction. Relevant elements are presented in red. Elements labeled with yellow color correspond to contaminants from sample sputter coating and SEM microscope environment
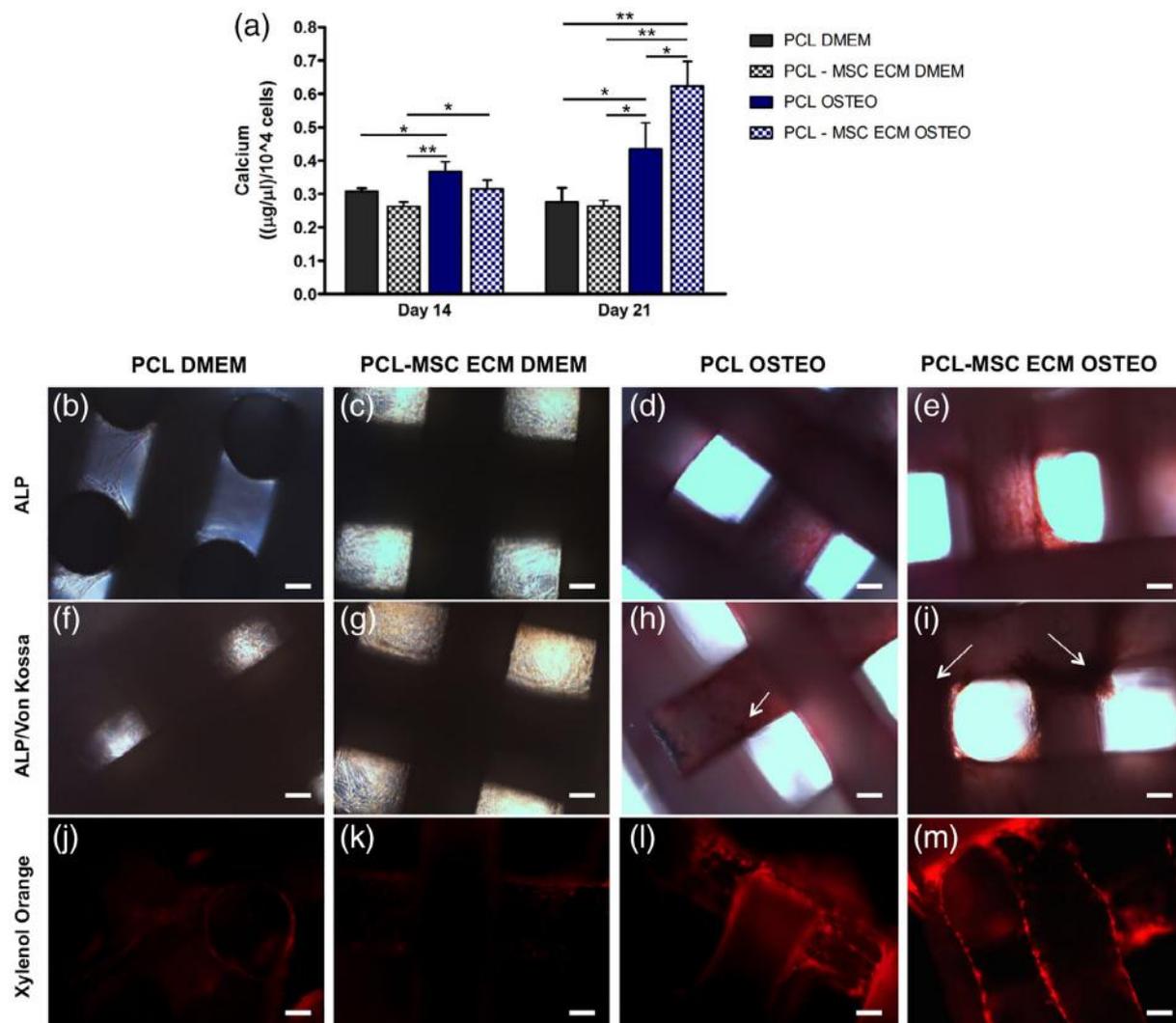
FIGURE 7 Osteogenic differentiation of MSC cultured on PCL-MSC ECM scaffolds. (a) Calcium deposition quantification assay of MSC seeded on PCL-MSC ECM and pristine PCL scaffolds after 14 and 21 days culture under osteogenic differentiation medium and standard expansion medium. Results are expressed as mean ± SD; n = 3; *p < .05, **p < .01. (b–e) ALP, (f–i) ALP/Von Kossa and (j–m) Xylenol Orange osteogenic stainings of MSC cultured for 21 days under osteogenic differentiation medium and standard expansion medium. ALP staining confirms ALP activity of cells by a red staining. Von Kossa evaluates the presence of calcium deposits (dark areas highlighted by the white arrows). Xylenol Orange fluorescent staining further confirms the presence of calcium deposits, which stain in red. Scale bar 100 μm

shown by SEM images/EDX spectrograms (Figure 6), Von Kossa (Figure 7f–i) and Xylenol Orange (Figure 7j-m) stainings.

4 | DISCUSSION

As an alternative to the standard treatment based on autologous and allogeneic bone grafts, scaffolds fabricated with different materials, such as polymers and ceramics, have been used in tissue engineering strategies to promote bone repair (Hasan et al., 2018). The majority of these constructs lack functionality and require the use of surface modification techniques to improve scaffold bioactivity and osteo-inductive properties. However, such approaches may affect scaffold structure and often fail to recapitulate the molecular complexity of the native bone ECM (Benders et al., 2013; Pati et al., 2015). Tissue-derived ECM of decellularized tissues or organs was proposed as a potential scaffold for BTE because of its higher molecular and structural complexity. However, limitations such as its scarcity, the risk of potential pathogen transfer, inflammatory responses, uncontrollable degradation kinetics, and weak mechanical properties have limited its use (Badylak, Freytes, & Gilbert, 2009; Cheng et al., 2014; Zhang et al., 2016).

In contrast, cell-derived ECM can be obtained from the in vitro culture of autologous cells, thereby overcoming the bottlenecks of tissue-derived ECM. Additionally, cell-derived ECM can be easily tailored to a specific application as it can be obtained from different cell types or blended with other materials. Therefore, the use of cell-derived ECM integrated with biomaterial scaffolds has appeared as a promising strategy for BTE applications (Fitzpatrick & McDevitt, 2015; Zhang et al., 2016). In this study, we combine additive

manufacturing technology with the concept of decellularized ECM to generate cell-derived ECM polymer-based scaffolds with a defined structure and enhanced bioactivity and osteoinductive properties. Our hypothesis is that by providing a close mimicry of the native bone niche, through the incorporation of MSC-derived ECM, it is possible to improve MSC osteogenic differentiation while maintaining the advantages of polymeric scaffolds such as a controlled and defined structure and good mechanical support.

PCL scaffolds used in this work were produced by FDM with controlled size and architecture (pore size of 390 μm/ 0–90° lay-down pattern). These scaffolds are previously characterized as presenting a high porosity (56.6%), high interconnectivity (99.7%), and a compressive modulus of 30 MPa (Silva et al., 2017). Similar PCL scaffolds, fabricated using the same AM technique, have been tested for BTE using MG-63 cells (Patrício, Domingos, Gloria, & Bártolo, 2014) and hBMSC (Endres et al., 2003). However, the performance of the PCL scaffold was limited by the suboptimal biological interaction between cells and synthetic material. Herein, we aimed to improve this interaction through the decoration of the PCL scaffold with MSC-derived ECM. After this decoration with decellularized MSC-ECM, no apparent changes in scaffold architecture were observed by SEM analysis, suggesting that the appropriate mechanical properties of the support were maintained. Accordingly, a previous study performed with PCL scaffolds fabricated by selective laser sintering showed no significant effect of 2 weeks cell culturing on the scaffold's compressive modulus (Eosoly, Vrana, Lohfeld, Hindie, & Looney, 2012).

The deposition of MSC-derived ECM on PCL scaffolds was confirmed by SEM and EDX analysis and by immunofluorescence staining of relevant ECM proteins. Because of their important role in promoting cell attachment, growth, and differentiation, fibronectin and laminin were selected as biomarkers for the presence of ECM on the scaffolds (Kleinman, Philp, & Hoffman, 2003; Matsubara et al., 2004). Positive immunofluorescent staining for fibronectin and laminin was clearly observed in PCL-MSC ECM scaffolds, however, staining associated with these two proteins was not homogeneously spread along the scaffold microfibers. A similar observation was made by Kim and colleagues, when assessing fibronectin distribution in human lung fibroblasts-derived ECM coated poly lactic-co-glycolic acid (PLGA)/PLA mesh scaffolds (Kim et al., 2015). SEM micrographs and EDX spectra analyzed in comparison with the ones obtained for the pristine PCL scaffold, further demonstrated the presence of deposited ECM on PCL-MSC ECM scaffolds. The presence of a nitrogen peak after decellularization in the PCL-MSC ECM scaffolds is in accordance with previous studies using bone-derived ECM or rat BMSC-derived ECM to enhance the biological performance of polymeric/ceramic scaffolds, respectively (Kim et al., 2017; Kim et al., 2018).

PCL-MSC ECM scaffolds enhanced significantly cell attachment and proliferation when compared with pristine PCL scaffolds, both under standard expansion and osteogenic induction. Previous studies have also shown increased cell numbers as a result of decellularized ECM incorporation in biomaterial scaffolds (Harvestine et al., 2016; Kim et al., 2015; Kim et al., 2017; Noh et al., 2016; Pati et al., 2015). In fact, Kim and collegues showed improved proliferation of

MC3T3-E1 osteoblast cells when cultured in rat BMSC-derived ECM coated biphasic calcium phosphate scaffolds (Kim et al., 2017), while Noh and colleagues reported higher umbilical cord blood-derived MSC cell numbers when cultured in a PLGA/PLA mesh scaffold coated with cell-derived ECM deposited by type I collagen over-expressing cells (Noh et al., 2016). This enhancing effect in cell proliferation might be explained by the presence of bioactive molecules such as growth factors and cytokines within or recruited by the deposited decellularized-ECM. Recent proteomic studies have demonstrated the presence of adhesive molecules and growth factor binding proteins in cell-derived ECM generated from BMSC (Ragelle et al., 2017). Moreover, fibroblast growth factor-2, which was shown to promote proliferation of adult BMSC, was also identified in decellularized cartilage-ECM (Rothrauff, Yang, & Tuan, 2017; Solchaga, Penick, Goldberg, Caplan, & Welter, 2010). This evidence is in accordance with our observations and might provide an explanation for the higher hBMSC proliferative potential obtained in PCL-MSC ECM scaffolds. Interestingly, hBMSC cultured on PCL-MSC ECM scaffolds under expansion medium showed a statistically significant increase in cell numbers at day 7 and 14 when compared to cells cultured on the same scaffolds (PCL-MSC ECM scaffolds) under osteogenic differentiation medium. In fact, different studies have reported the observation of specific changes in cell metabolism during differentiation (Klontzas, Vernardis, Heliotis, Tsiridis, & Mantalaris, 2017; Martano et al., 2019). Moreover, when committed toward the osteogenic lineage, MSC showed reduced metabolic activity and proliferation. Accordingly, Datta and colleagues observed decreased cell numbers over time, when rat marrow stromal cells were cultured in cell-derived ECM titanium constructs under osteogenic induction in comparison to the constructs cultured in standard expansion medium (Datta et al., 2005). Thus, the decreased cell numbers observed for PCL-MSC ECM OSTEO group in comparison to PCL-MSC ECM DMEM might be explained by a reduced cell metabolic activity during osteogenic differentiation.

Gene expression analysis supported the role of MSC-ECM on hBMSC osteogenic differentiation as verified by the upregulation of bone-specific marker genes. Regarding *COL I* and *Runx2* expression, this effect was predominant enough that hBMSC cultured in PCL-MSC ECM scaffolds without osteogenic supplementation presented significantly higher expressions than the ones cultured in PCL scaffolds under osteogenic induction. However, despite some signs of hBMSC osteogenic differentiation provided by the calcium production and mineralized nodules observed in PCL-MSC ECM DMEM group, the levels were considerably lower than the ones obtained for scaffolds cultured in osteogenic medium. In fact, *Runx2* is an early bone differentiation marker, and its expression is upregulated in immature osteoblasts and downregulated in mature osteoblasts because it is not essential to maintain the expression of the major bone matrix protein genes (Komori, 2009). Therefore, it is possible that osteogenic supplementation induced a later MSC osteogenic differentiation stage, explaining the lower *Runx2* expression in PCL-MSC ECM and PCL scaffolds after 21 days of culture in osteogenic medium. The significantly higher *OPN* expression observed for PCL-MSC ECM scaffolds

cultured under osteogenic induction compared to all other experimental groups, and more importantly the higher calcium content measured for this condition at day 21 of culture, suggest that a synergistic effect of PCL-MSC ECM scaffolds and osteogenic supplementation is important for a more mature MSC osteoblast differentiation state. Similar trends in *OPN* expression were previously reported when comparing cell-derived ECM coated PCL/PLGA scaffolds with their pristine PCL/PLGA scaffold counterparts (Pati et al., 2015). Moreover, we believe that the observed upregulation of *OPN* gene expression in PCL-MSC ECM scaffolds cultured in osteogenic media is stimulating mineralization. In fact, previous studies have already reported the inductive effect of *OPN* on mineralization (Boskey, 1995; Gericke et al., 2005; Zurick, Qin, & Bernards, 2013).

Our results suggest a positive role of MSC-derived ECM decoration of PCL scaffolds in hBMSC osteogenic differentiation. Qualitative osteogenic staining showed clearly higher ALP activity and calcium deposition when both scaffold types were cultured under osteogenic medium, confirming the results observed for *ALP* gene expression and calcium content. However, substantial differences between these were not observed, which is in accordance with previous studies that reported similar qualitative observations of the osteogenic stainings between ECM-derived and non-ECM scaffolds (Kim et al., 2017; Pati et al., 2015). In terms of calcium deposition by cells, all scaffolds promoted calcium production and no significant differences were observed between PCL-MSC ECM and pristine PCL scaffolds when cultured in standard expansion medium, with nearly constant values at all the time points assessed. Under osteogenic induction, both PCL-MSC ECM and PCL scaffolds promoted a significant increase in calcium production, however, a significant enhancement promoted by the MSC-ECM presence compared to pristine PCL was only observed after 21 days, which is in agreement with previously published data for BMSC cultured in different cell-derived ECM hybrid scaffold configurations (Kang, Kim, Khademhosseini, & Yang, 2011). In fact, the results of calcium quantification assay are concordant with the ones obtained from osteogenic staining, SEM analysis, and EDX spectra after 21 days of culture. SEM images suggest the presence of mineralized nodules in PCL-MSC ECM and PCL scaffolds cultured under osteogenic induction, which is supported by the identification of calcium element in the respective EDX spectrograms. In agreement, Fu and colleagues obtained similar results, in which they demonstrated the presence of mineralized modules after MSC osteogenic differentiation in both ECM-decorated poly-L-lactic acid (PLLA) and PLLA nanofiber mesh scaffolds (Fu, Liu, Cheng, & Cui, 2018). The mineralized nodules were also noticeable in lower abundance in PCL-MSC ECM scaffolds cultured under standard expansion conditions, suggesting a stimulatory effect of ECM in hBMSC osteogenesis, even in the absence of osteogenic supplementation. Such observation is in agreement with the work of Thibault and coworkers, which showed that the osteogenic differentiation of MSC cultured onto ECM-containing constructs was maintained even in the absence of dexamethasone (Thibault et al., 2010). Additionally, Datta and colleagues have also reported that MSC-derived ECM decoration of titanium scaffolds promotes the osteogenic differentiation of MSC, even in the absence of osteogenic supplements (Datta et al., 2006). However, our observations suggest that hBMSC osteogenic differentiation was enhanced by the synergistic effect of PCL-MSC ECM scaffolds and osteogenic induction medium, as supported by the elevated bone-specific markers gene expression and calcium levels. Thus, our results demonstrated that PCL-MSC ECM scaffolds presented a beneficial effect on MSC osteogenic differentiation and, therefore, are promising for being applied in personalized BTE strategies.

5 | CONCLUSIONS

In summary, we successfully established a method to fabricate 3D MSC-derived ECM-decorated porous PCL scaffolds with a defined structure and enhanced biological performance. The presence of ECM components on the PCL scaffold was confirmed by SEM/EDX and immunofluorescence analysis. PCL-MSC ECM scaffolds significantly promoted cell proliferation both under standard expansion and osteogenic differentiation conditions. The decellularized PCL-MSC ECM scaffolds showed improved osteoinductive properties, as clearly supported by the significantly higher calcium deposition and osteogenic relative gene expressions, particularly the higher expression of the osteogenic marker *OPN*, observed at day 21 when compared to pristine PCL scaffolds. This strategy, combining AM methods and decellularized ECM production, is promising for BTE applications as it allows the scalable fabrication of "patient-tailored" scaffolds that perfectly fit in the bone defect site, and possess enhanced bioactivity and osteoinductivity as a result of a closer mimicry of the native bone microenvironment.

CONFLICT OF INTEREST

The authors declare no conflict of interest.

REFERENCES

Badylak, S. F., Freytes, D. O., & Gilbert, T. W. (2009). Extracellular matrix as a biological scaffold material: Structure and function. *Acta Biomaterialia*, *5*, 1–13.

Benders, K. E. M., van Weeren, P. R., Badylak, S. F., Saris, D. B. F., Dhert, W. J. A., & Malda, J. (2013). Extracellular matrix scaffolds for cartilage and bone regeneration. *Trends in Biotechnology*, *31*, 169–176.

Boskey, A. L. (1995). Osteopontin and related phosphorylated Sialoproteins: Effects on mineralization. *Annals of the New York Academy of Sciences*, 760, 249–256.

Bracaglia, L. G., & Fisher, J. P. (2015). Extracellular matrix-based biohybrid materials for engineering compliant, matrix-dense tissues. *Advanced Healthcare Materials*, 4, 2475–2487.

Carvalho, M. S., Silva, J. C., Cabral, J. M. S., da Silva, C. L., & Vashishth, D. (2019). Cultured cell-derived extracellular matrices to enhance the osteogenic differentiation and angiogenic properties of human mesenchymal stem/stromal cells. *Journal of Tissue Engineering and Regenerative Medicine*, 13, 1544–1558.

Carvalho, M. S., Silva, J. C., Udangawa, R. N., Cabral, J. M. S., Ferreira, F. C., da Silva, C. L., … Vashishth, D. (2019). Co-culture cell-derived extracellular matrix loaded electrospun microfibrous scaffolds for bone tissue engineering. *Materials Science and Engineering: C*, 99, 479–490.

Cheng, C. W., Solorio, L. D., & Alsberg, E. (2014). Decellularized tissue and cell-derived extracellular matrices as scaffolds for orthopaedic tissue engineering. *Biotechnology Advances*, 32, 462–484.

Chiarello, E., Cadossi, M., Tedesco, G., Capra, P., Calamelli, C., Shehu, A., & Giannini, S. (2013). Autograft, allograft and bone substitutes in reconstructive orthopedic surgery. *Aging Clinical and Experimental Research*, 25, 101–103.

Choi, Y. C., Choi, J. S., Woo, C. H., & Cho, Y. W. (2014). Stem cell delivery systems inspired by tissue-specific niches. *Journal of Controlled Release*, 193, 42–50.

Datta, N., Holtorf, H. L., Sikavitsas, V. I., Jansen, J. A., & Mikos, A. G. (2005). Effect of bone extracellular matrix synthesized in vitro on the osteoblastic differentiation of marrow stromal cells. *Biomaterials*, 26, 971–977.

Datta, N., Pham, Q. P., Sharma, U., Sikavitsas, V. I., Jansen, J. A., & Mikos, A. G. (2006). In vitro generated extracellular matrix and fluid shear stress synergistically enhance 3D osteoblastic differentiation. *Proceedings of the National Academy of Sciences*, 103, 2488–2493.

Domingos, M., Chiellini, F., Gloria, A., Ambrosio, L., Bartolo, P., & Chiellini, E. (2012). Effect of process parameters on the morphological and mechanical properties of 3D bioextruded poly(ε-caprolactone) scaffolds. *Rapid Prototyping Journal*, 18, 56–67.

Endres, M., Hutmacher, D. W., Salgado, A. J., Kaps, C., Ringe, J., Reis, R. L., … Schantz, J. T. (2003). Osteogenic induction of human bone marrow-derived Mesenchymal progenitor cells in novel synthetic polymer–hydrogel matrices. *Tissue Engineering*, 9, 689–702.

Eosoly, S., Vrana, N. E., Lohfeld, S., Hindie, M., & Looney, L. (2012). Interaction of cell culture with composition effects on the mechanical properties of polycaprolactone-hydroxyapatite scaffolds fabricated via selective laser sintering (SLS). *Materials Science and Engineering C*, 32, 2250–2257.

Fernández-Pérez, J., & Ahearne, M. (2019). The impact of decellularization methods on extracellular matrix hydrogels. *Scientific Reports*, 9, 14993.

Fitzpatrick, L. E., & McDevitt, T. C. (2015). Cell-derived matrices for tissue engineering and regenerative medicine applications. *Biomaterials Science*, 3, 12–24.

Fu, Y., Liu, L., Cheng, R., & Cui, W. (2018). ECM decorated electrospun nanofiber for improving bone tissue regeneration. *Polymers*, 10, 272.

Gattazzo, F., Urciuolo, A., & Bonaldo, P. (2014). Extracellular matrix: A dynamic microenvironment for stem cell niche. *Biochimica et Biophysica Acta (BBA) - General Subjects*, 1840, 2506–2519.

Gericke, A., Qin, C., Spevak, L., Fujimoto, Y., Butler, W. T., Sørensen, E. S., & Boskey, A. L. (2005). Importance of phosphorylation for osteopontin regulation of biomineralization. *Calcified Tissue International*, 77, 45–54.

Gordeladze, J. O., Haugen, H. J., Lyngstadaas, S. P., & Reseland, J. E. (2017). Bone tissue engineering: State of the art, challenges, and prospects. In *Tissue engineering for artificial organs: Regenerative medicine, smart diagnostics and personalized medicine* (Vol. 2, pp. 525–551). Chennai, India: Wiley India Private Ltd.

Guler, Z., Silva, J. C., & Sezai Sarac, A. (2017). RGD functionalized poly (ε-caprolactone)/poly(m-anthranilic acid) electrospun nanofibers as high-performing scaffolds for bone tissue engineering RGD functionalized PCL/P3ANA nanofibers. *International Journal of Polymeric Materials and Polymeric Biomaterials*, 66, 139–148.

Hajiali, F., Tajbakhsh, S., & Shojaei, A. (2018). Fabrication and properties of polycaprolactone composites containing calcium phosphate-based ceramics and bioactive glasses in bone tissue engineering: A review. *Polymer Reviews*, 58, 164–207.

Harris, G. M., Raitman, I., & Schwarzbauer, J. E. (2018). Cell-derived decellularized matrices. *Methods in Cell Biology*, 143, 97–114.

Harvestine, J. N., Vollmer, N. L., Ho, S. S., Zikry, C. A., Lee, M. A., & Leach, J. K. (2016). Extracellular matrix-coated composite scaffolds promote Mesenchymal stem cell persistence and Osteogenesis. *Biomacromolecules*, 17, 3524–3531.

Hasan, A., Byambaa, B., Morshed, M., Cheikh, M. I., Shakoor, R. A., Mustafy, T., & Marei, H. E. (2018). Advances in osteobiologic materials for bone substitutes. *Journal of Tissue Engineering and Regenerative Medicine*, 12, 1448–1468.

Holmes, D. (2017). Non-union bone fracture: A quicker fix. *Nature*, 550, S193.

Hoshiba, T., Lu, H., Kawazoe, N., & Chen, G. (2010). Decellularized matrices for tissue engineering. *Expert Opinion on Biological Therapy*, 10, 1717–1728.

Hutmacher, D. W., Schantz, T., Zein, I., Ng, K. W., Teoh, S. H., & Tan, K. C. (2001). Mechanical properties and cell cultural response of polycaprolactone scaffolds designed and fabricated via fused deposition modeling. *Journal of Biomedical Materials Research*, 55, 203–216.

Hynes, R. O. (2009). The extracellular matrix: Not just pretty fibrils. *Science*, 326, 1216–1219.

Kang, Y., Kim, S., Bishop, J., Khademhosseini, A., & Yang, Y. (2012). The osteogenic differentiation of human bone marrow MSCs on HUVEC-derived ECM and β-TCP scaffold. *Biomaterials*, 33, 6998–7007.

Kang, Y., Kim, S., Khademhosseini, A., & Yang, Y. (2011). Creation of bony microenvironment with CaP and cell-derived ECM to enhance human bone-marrow MSC behavior and delivery of BMP-2. *Biomaterials*, 32, 6119–6130.

Kim, B., Ventura, R., & Lee, B. T. (2017). Functionalization of porous BCP scaffold by generating cell-derived extracellular matrix from rat bone marrow stem cells culture for bone tissue engineering. *Journal of Tissue Engineering and Regenerative Medicine*, 12, 1256–1267.

Kim, I. G., Hwang, M. P., Du, P., Ko, J., Ha, C.-W., Do, S. H., & Park, K. (2015). Bioactive cell-derived matrices combined with polymer mesh scaffold for osteogenesis and bone healing. *Biomaterials*, 50, 75–86.

Kim, J.-Y., Ahn, G., Kim, C., Lee, J.-S., Lee, I.-G., An, S.-H., … Shim, J. H. (2018). Synergistic effects of Beta tri-calcium phosphate and porcine-derived Decellularized bone extracellular matrix in 3D-printed Polycaprolactone scaffold on bone regeneration. *Macromolecular Bioscience*, 18, 1800025.

Kleinman, H. K., Philp, D., & Hoffman, M. P. (2003). Role of the extracellular matrix in morphogenesis. *Current Opinion in Biotechnology*, 14, 526–532.

Klontzas, M. E., Vernardis, S. I., Heliotis, M., Tsiridis, E., & Mantalaris, A. (2017). Metabolomics analysis of the osteogenic differentiation of umbilical cord blood mesenchymal stem cells reveals differential sensitivity to osteogenic agents. *Stem Cells and Development*, 26, 723–733.

Komori, T. (2009). *Regulation of osteoblast differentiation by runx2* (pp. 43–49). Boston, MA: *Osteoimmunology*. Springer.

Ku, Y., Chung, C. P., & Jang, J. H. (2005). The effect of the surface modification of titanium using a recombinant fragment of fibronectin and vitronectin on cell behavior. *Biomaterials*, 26, 5153–5157.

Kundu, A. K., & Putnam, A. J. (2006). Vitronectin and collagen I differentially regulate osteogenesis in mesenchymal stem cells. *Biochemical and Biophysical Research Communications*, 347, 347–357.

Lai, Y., Sun, Y., Skinner, C. M., Son, E. L., Lu, Z., Tuan, R. S., ... Chen, X.-D. (2010). Reconstitution of marrow-derived extracellular matrix ex vivo: A robust culture system for expanding large-scale highly functional human Mesenchymal stem cells. *Stem Cells and Development*, *19*, 1095–1107.

Low, S. W., Ng, Y. J., Yeo, T. T., & Chou, N. (2009). Use of Osteoplug polycaprolactone implants as novel burr-hole covers. *Singapore Medical Journal*, *50*, 777–780.

Martano, G., Borroni, E. M., Lopci, E., Cattaneo, M. G., Mattioli, M., Bachi, A., ... Bifari, F. (2019). Metabolism of stem and progenitor cells: Proper methods to answer specific questions. *Frontiers in Molecular Neuroscience*, *12*, 151.

Matsubara, T., Tsutsumi, S., Pan, H., Hiraoka, H., Oda, R., Nishimura, M., ... Kato, Y. (2004). A new technique to expand human mesenchymal stem cells using basement membrane extracellular matrix. *Biochemical and Biophysical Research Communications*, *313*, 503–508.

Melchels, F. P. W., Domingos, M. A. N., Klein, T. J., Malda, J., Bartolo, P. J., & Hutmacher, D. W. (2012). Additive manufacturing of tissues and organs. *Progress in Polymer Science*, *37*, 1079–1104.

Mota, C., Puppi, D., Chiellini, F., & Chiellini, E. (2015). Additive manufacturing techniques for the production of tissue engineering constructs. *Journal of Tissue Engineering and Regenerative Medicine*, *9*, 174–190.

Neves, L. S., Rodrigues, M. T., Reis, R. L., & Gomes, M. E. (2016). Current approaches and future perspectives on strategies for the development of personalized tissue engineering therapies. *Expert Review of Precision Medicine and Drug Development*, *1*, 93–108.

Noh, Y. K., Du, P., Kim, I. G., Ko, J., Kim, S. W., & Park, K. (2016). Polymer mesh scaffold combined with cell-derived ECM for osteogenesis of human mesenchymal stem cells. *Biomaterials Research*, *20*, 6.

Pati, F., Song, T. H., Rijal, G., Jang, J., Kim, S. W., & Cho, D. W. (2015). Ornamenting 3D printed scaffolds with cell-laid extracellular matrix for bone tissue regeneration. *Biomaterials*, *37*, 230–241.

Patrício, T., Domingos, M., Gloria, A., & Bártolo, P. (2014). Fabrication and characterisation of PCL and PCL/PLA scaffolds for tissue engineering. *Rapid Prototyping Journal*, *20*, 145–156.

Poh, P. S. P., Hutmacher, D. W., Holzapfel, B. M., Solanki, A. K., Stevens, M. M., & Woodruff, M. A. (2016). In vitro and in vivo bone formation potential of surface calcium phosphate-coated polycaprolactone and polycaprolactone/bioactive glass composite scaffolds. *Acta Biomaterialia*, *30*, 319–333.

Ragelle, H., Naba, A., Larson, B. L., Zhou, F., Prijić, M., Whittaker, C. A., ... Anderson, D. G. (2017). Comprehensive proteomic characterization of stem cell-derived extracellular matrices. *Biomaterials*, *128*, 147–159.

Roseti, L., Parisi, V., Petretta, M., Cavallo, C., Desando, G., Bartolotti, I., & Grigolo, B. (2017). Scaffolds for bone tissue engineering: State of the art and new perspectives. *Materials Science and Engineering C*, *78*, 1246–1262.

Rothrauff, B. B., Yang, G., & Tuan, R. S. (2017). Tissue-specific bioactivity of soluble tendon-derived and cartilage-derived extracellular matrices on adult mesenchymal stem cells. *Stem Cell Research & Therapy*, *8*, 133.

Schantz, J. T., Lim, T. C., Ning, C., Swee, H. T., Kim, C. T., Shih, C. W., & Hutmacher, D. W. (2006). Cranioplasty after trephination using a novel biodegradable burr hole cover: Technical case report. *Operative Neurosurgery*, *58* ONS-E176. http://www.spartanmedspine.com/files/Cranioplasty-after-Trephination-using-Osteoplug.pdf

Silva, J. C., Moura, C. S., Alves, N., Cabral, J. M. S., & Ferreira, F. C. (2017). Effects of different fibre alignments and bioactive coatings on mesenchymal stem/stromal cell adhesion and proliferation in poly (ε-caprolactone) scaffolds towards cartilage repair. *Procedia Manufacturing*, *12*, 132–140.

Solchaga, L. A., Penick, K., Goldberg, V. M., Caplan, A. I., & Welter, J. F. (2010). Fibroblast growth Factor-2 enhances proliferation and delays loss of Chondrogenic potential in human adult bone-marrow-derived Mesenchymal stem cells. *Tissue Engineering Part A*, *16*, 1009–1019.

Thibault, R. A., Scott Baggett, L., Mikos, A. G., & Kasper, F. K. (2010). Osteogenic differentiation of Mesenchymal stem cells on Pregenerated extracellular matrix scaffolds in the absence of Osteogenic cell culture supplements. *Tissue Engineering Part A*, *16*, 431–440.

Tour, G., Wendel, M., & Tcacencu, I. (2011). Cell-derived matrix enhances Osteogenic properties of hydroxyapatite. *Tissue Engineering Part A*, *17*, 127–137.

Won, J.-E., Mateous-Timoneda, M. A., Castano, O., Planell, J. A., Seo, S.-J., Lee, E.-J., ... Kim, H.-W. (2015). Fibronectin immobilization on to robotic-dispensed nanobioactive glass/polycaprolactone scaffolds for bone tissue engineering. *Biotechnology Letters*, *37*, 935–942.

Zhang, W., Zhu, Y., Li, J., Guo, Q., Peng, J., Liu, S., ... Wang, Y. (2016). Cell-derived extracellular matrix: Basic characteristics and current applications in orthopedic tissue engineering. *Tissue Engineering Part B: Reviews*, *22*, 193–207.

Zurick, K. M., Qin, C., & Bernards, M. T. (2013). Mineralization induction effects of osteopontin, bone sialoprotein, and dentin phosphoprotein on a biomimetic collagen substrate. *Journal of Biomedical Materials Research - Part A*, *101*, 1571–1581.